Am J Transl Res 2019;11(9):5836-5846
www.ajtr.org /ISSN:1943-8141/AJTR0099521

Original Article

BCOR-CCNB3 fusion and *BCOR* internal tandem duplication in undifferentiated round cell sarcoma: a pathologic and molecular study of 5 cases

Yang Yang*, Huijuan Shi*, Jiaxin Zheng, Huabin Gao, Tiantian Zhen, Fenfen Zhang, Anjia Han

*Department of Pathology, The First Affiliated Hospital, Sun Yat-sen University, Guangzhou 510080, Guangdong, P. R. China. *Equal contributors.*

Received July 11, 2019; Accepted July 26, 2019; Epub September 15, 2019; Published September 30, 2019

Abstract: Undifferentiated round cell sarcomas (URCSs) usually remained unclassified due to lack of known genetic abnormalities. Herein, we retrospectively collected 5 cases of URCSs and sought to investigate their unique clinicopathologic and molecular features for providing more accurate classification. There were 2 males and 3 females with age ranged from 7 months to 17 years. The tumors were respectively located in the sacrum, fibula, neck, perineum or groin. Microscopically, all 5 tumors were composed of small-to-medium sized cells with primitive morphology and variable cellularity, distributed within loose myxoid or collagenized fibroid stroma. These tumors lacked specific immunophenotypes and known gene rearrangements. However, the expression levels of CD99 and cyclin D1 were variable. RNA-sequencing data identified one *BCOR-CCNB3* gene fusion-positive sarcoma occurring in the sacrum of a 17-year-old male patient. Whole genome sequencing analysis detected *BCOR* exon 15-internal tandem duplication (*BCOR*-ITD) in the tumor arising in the groin of one 7-month-old female infant. No specific gene abnormalities were found in the other 3 cases. Interestingly, a morphological and immunohistochemical overlap existed between *BCOR*-rearrangement tumor and *BCOR*-ITD-positive tumor, including areas with hypercellularity alternating with hypocellularity, a mixture of round cells and focal spindle cells, pale nuclear chromatin, inconspicuous nucleoli and abundant myxoid matrix, diffuse strong cyclin D1 expression, relatively strong expression of CD99 but lower than that in Ewing sarcoma, and a low Ki-67 proliferation index of about 10%. Our findings demonstrated a significant link between genetic aberration and histopathologic appearances, thus supporting the crucial role of genetic characteristics in accurate clinicopathological classification.

Keywords: Undifferentiated round cell sarcomas (URCSs), *BCOR* internal tandem duplication (*BCOR*-ITD), *BCOR-CCNB3*

Introduction

Undifferentiated round cell sarcomas (URCSs) arising in soft tissues of children and young adults are highly aggressive tumors [1]. Most of URCSs are often diagnostically challenging, due to lack of known genetic abnormalities. With the advent of next-generation sequencing, an increasing number of soft tissue sarcomas classified as URCSs based solely on morphology and immunohistochemistry were found to display novel gene fusions and other types of abnormalities and then reclassified into new entities. Recently, Both *BCOR* rearrangements [2, 3] and *CIC* rearrangements [4-6] have been reported in a small number of tumors which display morphologic and immunophenotypic overlap with ES, but lack *EWSR1* or *FUS* rearrangements and thus are referred to as 'Ewing-like sarcoma' or 'atypical Ewing sarcoma'.

Herein, we investigated 5 round cell sarcomas arising in the bones and soft tissues which initially fell into the category of URCSs by whole transcriptome paired-end RNA sequencing (RNA-seq) and whole genome sequencing (WGS). Additionally, a case of Ewing sarcoma (ES) that had *EWSR1* rearrangement detected by FISH, was used as positive control to validate the utility and accuracy of RNA-seq.

Materials and methods

Case selection

Aiming for cases of similar histology, we selected patients younger than twenty years of age

(infants, children, and teenagers) and initially diagnosed as URCSs. A total of 5 URCSs were acquired between 2016 and 2018 at Department of Pathology, Sun Yat-sen University. A retrospective review was performed in these cases, including all the available clinicopathologic data, morphology, immunohistochemistry analyses, and break-apart fluorescent *in situ* hybridization (FISH) results. One case of ES showing *EWSR1* gene rearrangement was used as positive control. This study was approved by Institutional Review Board at Sun Yat-sen University.

Fluorescence in situ hybridization (FISH)

Dual color FISH was performed on interphase nuclei to identify the presence of some known gene rearrangements using *EWSR1*, *SYT* and *FUS* break-apart probes (Vysis LSI® EWSR1 (22q12) Dual Color, Break Apart Rearrangement Probe; Vysis LSI® SS18 (18q11.2) Dual Color, Break Apart Rearrangement Probe; Vysis LSI® FUS (16p11) Dual Color, Break Apart Rearrangement Probe). Detailed information can be acquired in Supplementary Protocols.

RNA sequencing (RNA-seq) and fusion detection

Total RNA was extracted using RNeasy FFPE kit (Qiagen, Hilden, Germany) from FFPE samples. Ribosomal RNA was depleted using RNase H followed by library preparation using KAPA Stranded RNA-seq Kit with RiboErase (HMR) (KAPA Biosystems). The library concentration was determined by KAPA Library Quantification Kit (KAPA Biosystems), and the library quality was accessed by Agilent High Sensitivity DNA kit (Agilent Technologies, Santa Clara, CA) on Agilent 2100 Bioanalyzer (Agilent Technologies). Then, the library was sequenced on Illumina HiSeq NGS platforms (Illumina, San Diego, CA). Three tools including FusionCatcher, Factera and Socrates were applied for fusion detection of RNA-seq data. See Supplementary Protocols for details.

Whole genome sequencing (WGS)

Genomic DNA from FFPE sample was extracted and sequencing libraries were prepared. Then, Library fragment was sequenced on HiSeqX-TEN NGS platforms (Illumina) according to the manufacturer's instructions. See Supplementary Protocols for details.

Results

Clinicopathologic characteristics of 5 URCSs

A concise summary of the clinicopathologic features for 5 cases of URCSs was shown in **Table 1**. There were 2 males and 3 females. The median age at diagnosis of all the patients was 1 years (range, 7 months to 17 years, mean 6.1 years). The tumors occurred in the bones (sacrum and fibula) and somatic soft tissues (neck, perineum and groin). The tumor size was available for 3 patients and ranged from 2 to 5 cm (mean, 3.2 cm) in the largest dimension. At initial diagnosis, 3 patients had localized disease without evidence of metastasis, while relevant information was unavailable in another 2 patients.

Microscopically, all 5 tumors were composed of small-to-medium sized cells with variable degrees of cellularity, primitive morphology and mild pleomorphism, accompanied by a well-developed vasculature. At low magnification, case 1 and case 3 showed solid sheets of densely packed neoplastic cells (**Figure 1A** and **1E**). Case 2 and case 4 were composed of areas with hypercellularity alternated with hypocellularity (**Figure 1C** and **1G**). In areas with high cellularity, the tumor cells showed a sheet-like growth pattern, while in less cellular areas, the discohesive tumor cells were distributed within loose myxoid matrix. Variable degree of myxoid stromal change was noted in all the cases. A small amount of fibrous stroma was presented in four cases, while abundant collagenized fibrous stroma was only seen in case 5 (**Figure 1I**). Case 5 exhibited alternating collagenized and myxoid areas. In the dense collagenized stroma, the tumor cells were arranged in nests or cords-like growth pattern, while in the loose myxoid matrix, the tumor cells were distributed scatteredly. In 5 URCSs, the tumor cells were mostly round-to-ovoid with clear or eosinophilic cytoplasm and finely stippled nuclear chromatin. The nuclei of the tumor cells in case 1 (**Figure 1B**) and case 3 (**Figure 1F**) were vesicular with occasional punctate nucleoli, while the tumor cell nuclei displayed pale chromatin and inconspicuous nucleoli in case 2 (**Figure 1D**) and case 4 (**Figure 1H**). Case 5 was composed of monotonous small blue round cells with scant cytoplasm and hyperchromatic nuclei (**Figure 1J**). All 5 cases were mitotically active and the mean mitotic

Table 1. Clinical features and pathological characteristics of the 5 cases of URCSs and one case of ES

Case No.	Age/Sex	Primary site	Size (cm)	Sample source	Stage	Metastatic site	Microscopic Findings				
							Histologic Structure	Cytomorphology	Nuclear Features	Mitotic Count	Tumor Stroma
1	11 y/F	Neck	2.5	Resection	L	NEM	Solid sheet-like growth pattern	Round to oval	Vesicular nuclei with finely dispersed chromatin and occasional small nucleoli	10	Focal myxoid change
2	17 y/M	Sacrum	N/A	Biopsy	N/A	N/A	Hypercellularity alternating with hypocellularity, with a sheet-like growth pattern in hypercellular areas and a loose cellular distribution in hypocellular areas	Round cells blended with spindle cell components arranged in fascicles or whirlpools	Round-to-ovoid nuclei with pale chromatin and indistinct nucleoli	10	Extensive myxoid change
3	1 y/F	perineum	5	Resection	L	NEM	Solid sheet-like growth pattern	Round to oval	Vesicular nuclei with finely dispersed chromatin and occasional small nucleoli	30	Extensisve myxoid change
4	7 m/F	Groin	N/A	Biopsy	N/A	N/A	Hypercellularity alternating with hypocellularity, with a sheet-like growth pattern in hypercellular areas and a loose cellular distribution in hypocellular areas	Round cells blended with spindle cell components arranged in fascicles or whirlpools	Round-to-ovoid nuclei with pale chromatin and indistinct nucleoli	20	Extensive myxoid change and microcyst formation
5	1 y/M	fibula	2	Biopsy	L	NEM	Alternating dense and loose areas, with a nests or cords-like cellular growth pattern in dense collagenous areas, and a scatter cellular distribution in loose myxoid areas	Monotonous small blue round cells with scant cytoplasm	Hyperchromatic nuclei with inconspicuous nucleoli	25	Alternating collagenized and myxoid areas
Control case (ES)	9 y/F	ilium	N/A	Biopsy	L	NEM	Neoplastic cells arranged in sheets or cords	Undifferentiated small blue round cells with scant cytoplasm	Hyperchromatic nuclei with inconspicuous nucleoli	5	Thick collagenous bands

Abbreviations: URCSs, undifferentiated round cell sarcomas; ES, Ewing sarcoma; y, years; m, months; F, Female; M, Male; L, Localized disease; N/A, Not applicable; NEM, No evidence of metastasis.

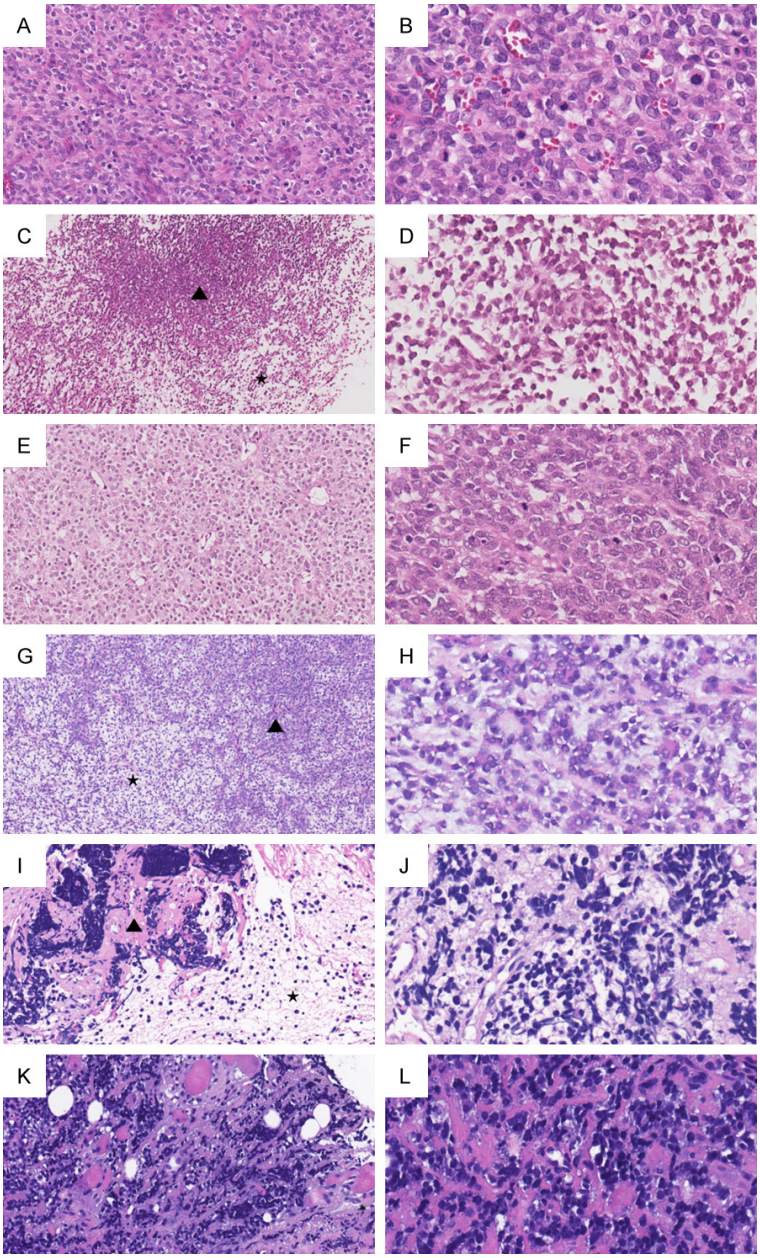

Figure 1. Histomorphology of the 5 URCSs and 1 ES. (A, B) Case 1. Morphology appearance showed diffuse sheets of densely packed neoplastic cells (A, 200×), with vesicular nuclei, occasional punctate nucleoli and common mitoses (B, 400×). (C, D) Case 2. The tumor was comprised of hypercellularity areas (triangle) alternating with hypocellularity areas (star) (C, 100×). The neoplastic cells had ovoid nuclei with pale chromatin and indistinct nucleoli (D, 400×). (E, F) Case 3. Diffuse sheets of tumor cells with a delicate thin-walled vascular network (E, 200×); vesicular nuclei with occasional small nucleoli and brisk mitotic activity (F, 400×). (G, H) Case 4. The tumor was comprised of areas with high cellularity (triangle) alternating with less cellular areas (star) (G, 100×). The tumor cells displayed eosinophilic cytoplasm, pale nuclear chromatin and inconspicuous nucleoli (H, 400×). (I, J) Case 5. The tumor was consisted of dense (triangle) and loose (star) areas (I, 200×). The tumor cells exhibited the morphology of monotonous small blue round cells with scant cytoplasm and hyperchromatic nuclei (J, 400×). (K, L) Histology of the control case (ES). Diffuse sheets of small blue round cells infiltrated into skeletal muscle and adipose tissue (K, 200×). The neoplastic cells with scant cytoplasm, hyperchromatic nuclei, and indistinct nucleoli were distributed within collagenized fibrous stroma (L, 400×).

rate was 19 mitoses per 10 high-power fields (range, 10-30/10 HPFs). Additionally, we observed short spindle tumor cells forming fascicles or whirlpools in focal areas of case 2 (**Figure 2A**, **2C** and **2E**) and case 4 (**Figure 2B**, **2D** and **2F**). A delicate arborizing vascular network (**Figure 2G**), extensive myxoid matrix with evident microcyst formation (**Figure 2H**), and cellular fibrous septa (**Figure 2I**) were in particular noted in case 4, very similar to those seen in clear cell sarcoma of kidney (CCSK). Vascular pseudorosettes were observed in case 3 (Supplementary Figure 1) and foci of tumor necrosis were only found in case 5 (Supplementary Figure 2). In the control case (ES), the neoplastic cells displayed a destructive infiltration into skeletal muscle and adipose tissue (**Figure 1K**) and exhibited the classic morphologic features of the small blue round tumor cells which were arranged in sheets or cords and surrounded by thick collagenous bands (**Figure 1L**).

The immunohistochemical findings were summarized in **Figure 3**. The levels of CD99 expression were variable in our cohort, which were relatively strongly positive in case 2 (**Figure 4B**) and case 4 (**Figure 4D**), moderately positive in case 3 (**Figure 4C**), and negative in case 1 (**Figure 4A**) and case 5 (**Figure 4E**). No one case showed diffuse and strong positivity for CD99 as that in the control case (**Figure 4F**). Nuclear cyclin D1 expression was observed in all 5 tumors but with varying extent and intensity (**Figure 4G-K**), being both diffuse and strong only in case 2 (**Figure 4H**) and case 4 (**Figure 4J**). Moreover, we noted

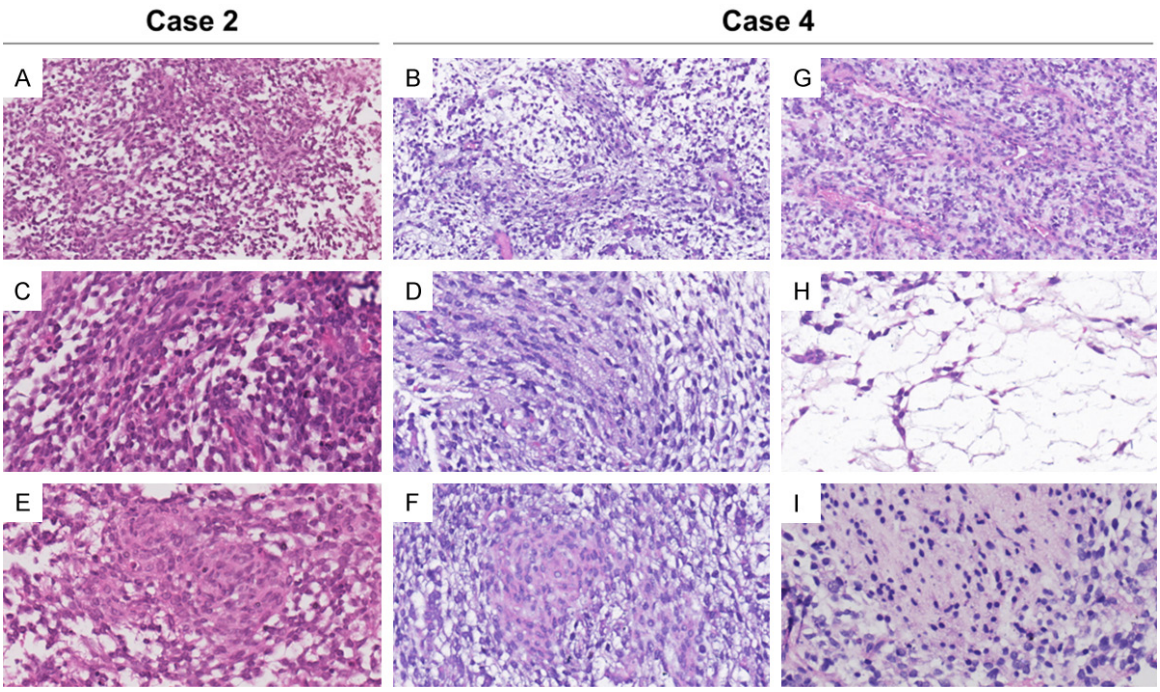

Figure 2. Additional histologic features in case 2 and case 4. (A, B) In focal areas of case 2 (A, 200×) and case 4 (B, 200×), the round cell components blended with the short spindle-shaped cells (200×). (C, D) The short spindle cells presented in case 2 (C, 400×) and case 4 (D, 400×) formed fascicular architecture. (E, F) The short spindle cells formed vortex-like structure in case 2 (E, 400×) and case 4 (F, 400×). (G) A delicate branching vasculature in case 4 (200×). (H) Abundant myxoid stroma and evident microcyst formation in case 4 (400×). (I) Cellular fibrous septa in case 4 (400×).

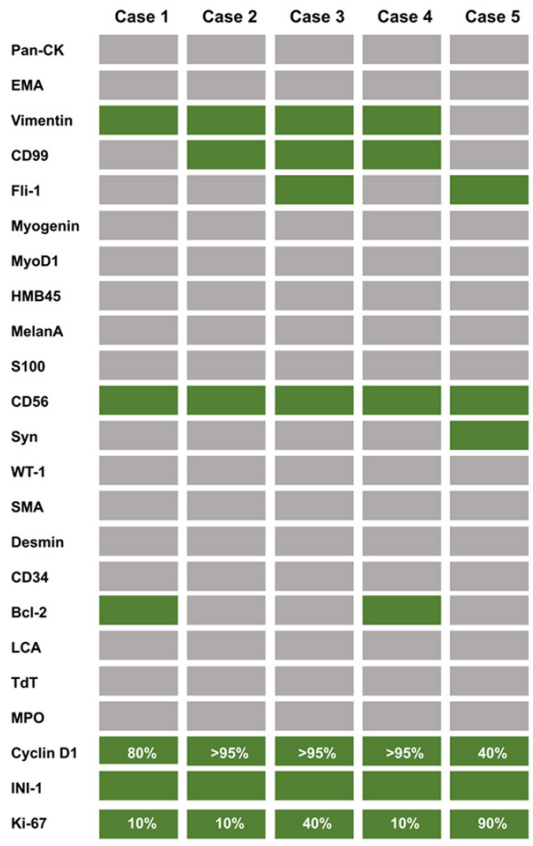

Figure 3. A summary of all the immunohistochemical findings for 5 cases of URCSs. Green, positive; gray, negative. pan-CK, pan-cytokeratin; EMA, epithelial membrane antigen; Syn, synaptophysin; WT-1, Wilms' tumour suppressor gene 1; SMA, smooth muscle actin; MPO, Myeloperoxidase; INI-1, SMARCB1 (SW1/SNF related, matrix associated, actin dependent regulator of chromatin B1). For cyclin D1 and Ki-67, the percentage of positive tumor cells was estimated.

that in case 1 cyclin D1 was highly expressed in perivascular tumor cells (**Figure 4G**). In control case (ES), strong cyclin D1 expression was simultaneously presented in nucleus and cytoplasm (**Figure 4L**). Immunostaining for CD56 was also seen in all 5 URCSs (**Figure 4M-Q**), of which case 2 (**Figure 4N**) and case 4 (**Figure 4P**) showed patchy and weak positivity and the remainder displayed diffuse positivity with moderate-to-strong intensity. Concurrent diffuse and strong staining of CD56 (**Figure 4Q**) and synaptophysin (**Figure 4R**) was only noted in case 5, suggesting neuroendocrine differentiation of this tumor. Fli-1 was only scatteredly positive in case 3 (Supplementary Figure 3A) and case 5 (Supplementary Figure 3B), where-

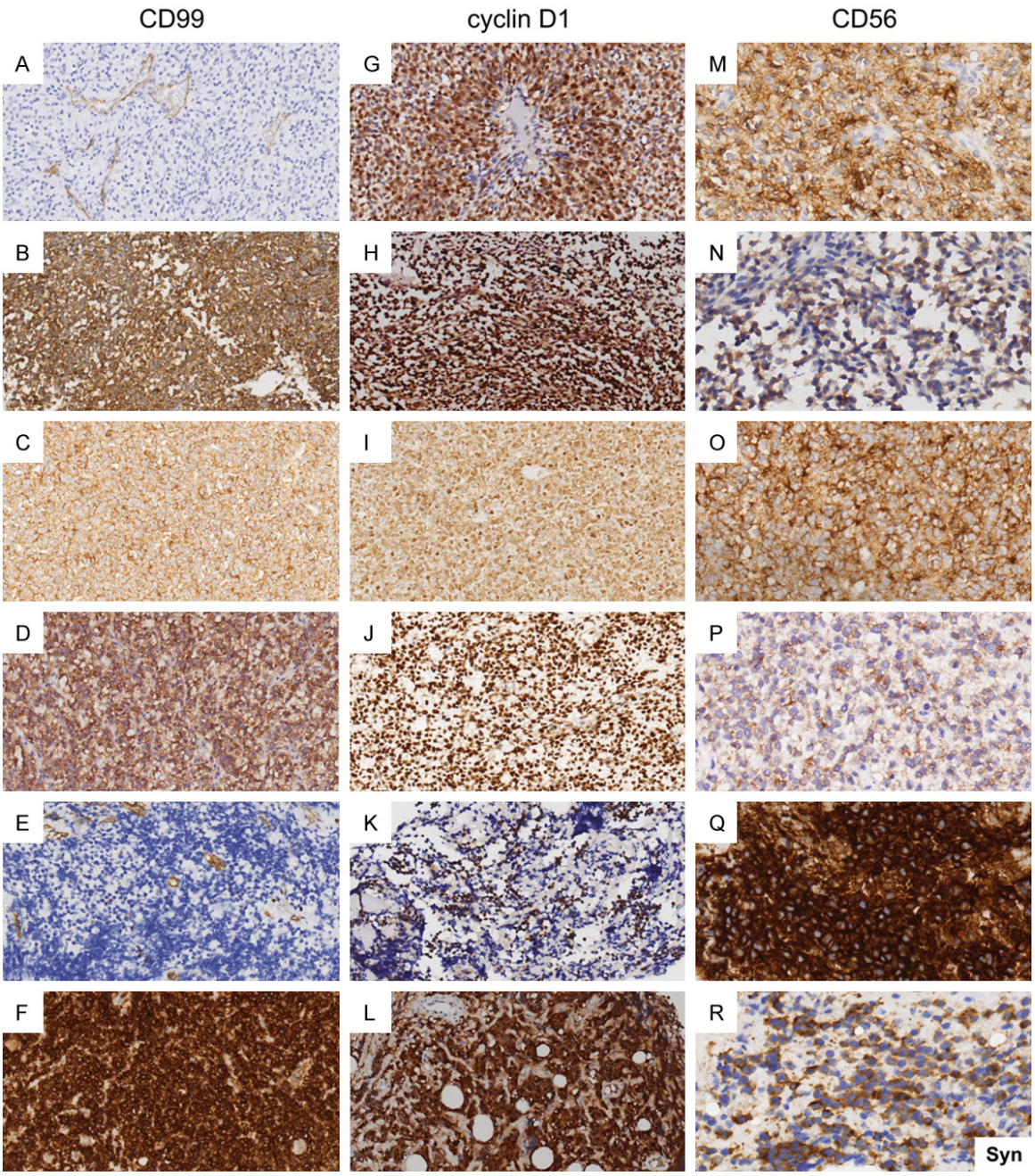

Figure 4. Representative images of immunohistochemical features in the 5 URCSs and 1 ES. (A, G and M) Case 1; (B, H and N) Case 2; (C, I and O) Case 3; (D, J and P) Case 4; (E, K, Q, and R) Case 5; (F, L) ES case. Membranous CD99 immunoreactivity was absent in case 1 (A) and case 5 (E), moderate in case 3 (C), and relatively strong in case 2 (B) and case 4 (D). CD99 expression in ES (F) was diffusely and strongly positive. Nuclear cyclin D1 expression was diffuse strong in case 2 (H) and case 4 (J), moderate in case 3 (I), and patchy in case 5 (K). Additionally in case 1 (G), cyclin D1 was more strongly expressed in perivascular areas, and in ES case (L), its strong expression was concurrently presented in nucleus and cytoplasm. Staining for CD56 exhibited patchy and weak positivity in case 2 (N) and case 4 (P), diffuse moderate in case 1 (M) and case 3 (O), while diffuse strong in case 5 (Q). Additionally, diffuse and strong synaptophysin positivity was also observed in case 5 (R). (A-L) 200× magnification; (M-R) 400× magnification.

as in ES case although Fli-1 was expressed in the most of tumor cells, its immunostaining was extremely weak (Supplementary Figure 3C). All cases were negative for pan-cytokeratin and EMA. In all 5 URCSs, the expression of INI-1 protein was retained in the nuclei of tumor cells. Staining of Ki-67 showed a low proliferation index in case 2 and case 4 (both with 10%

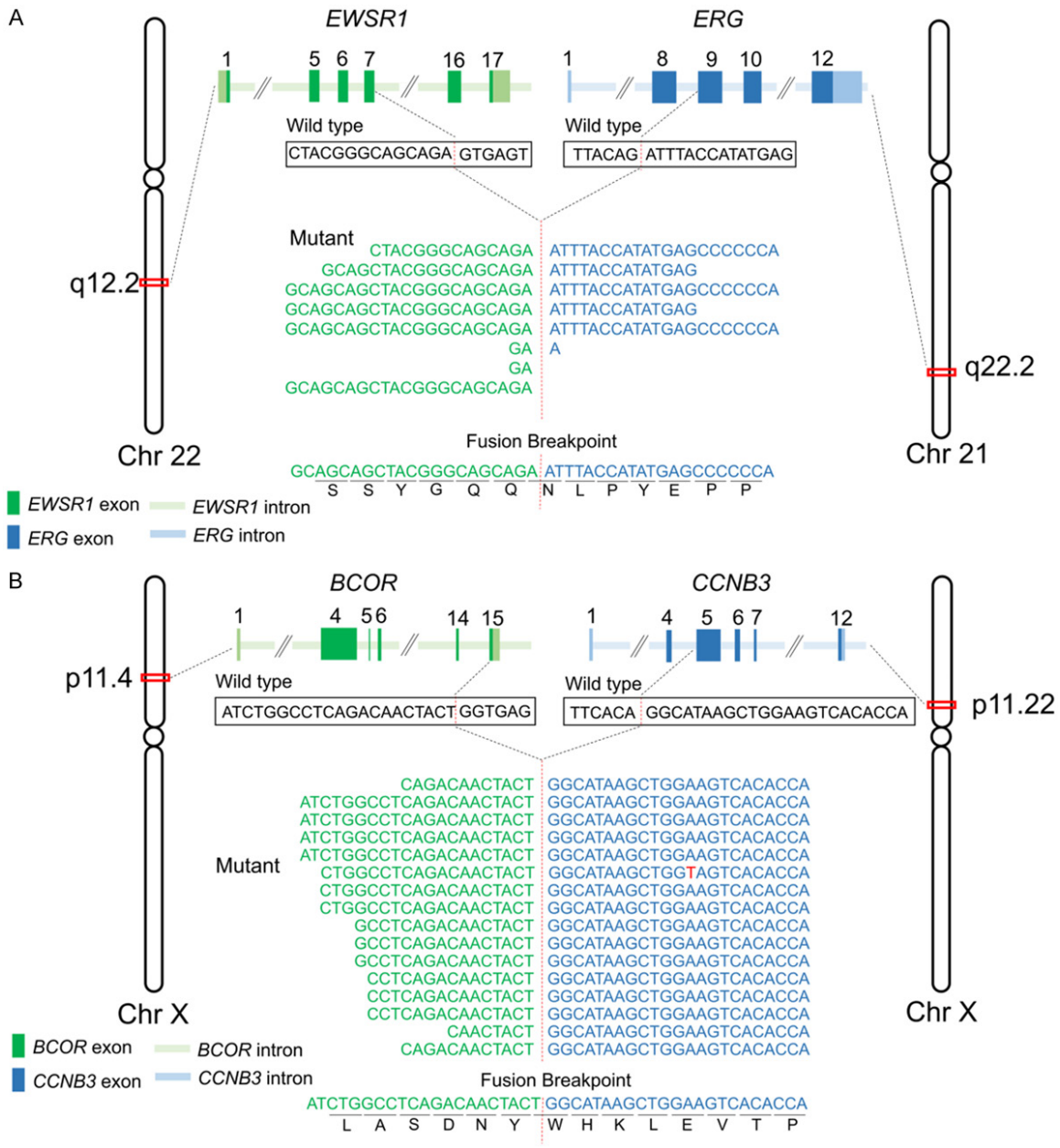

Figure 5. Fusion transcripts discovery by RNA-sequencing. (A) Schematic representation indicating *EWSR1-ERG* fusion (intron 7 of *EWSR1* on 22q12.2 fused to intron 8 of *ERG* on 21q22.2). (B) Schematic representation demonstrating *BCOR-CCNB3* fusion (exon 15 of *BCOR* on Xp11.4 fused to intron 4 of *CCNB3* on Xp11.22). In (A and B), alignment of the RNA reads covering the fusion junction are shown and the predicted amino acid sequence are displayed at the bottom of the schematic diagram. The fusion breakpoints are demarcated by red vertical dash lines.

nuclear labeling), while Ki-67 proliferation index was extremely high in case 5 and ES case (respectively up to 90% and 80%).

No known gene fusions including *EWSR1, FUS,* and *SYT,* were found using break-apart FISH in all 5 URCSs. However, *EWSR1* rearrangement was successfully detected in the control case (ES) by FISH analysis (Supplementary Figure 4).

Specific gene fusion transcripts or genetic abnormality in URCSs

We performed RNA-seq in all these cases. In control case, RNA-seq data successfully confirmed *EWSR1* gene rearrangement and identified a fusion transcript between *EWSR1* intron 7 and *ERG* intron 8 (**Figure 5A**). In case 2, RNA-seq analysis identified the junction between

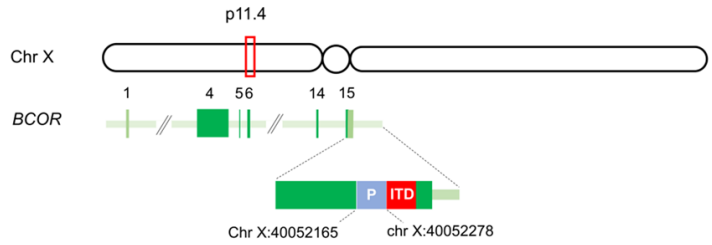

Figure 6. *BCOR* exon 15-internal tandem duplication in case 4. View of aligned whole genome sequencing reads from case 4 demonstrated the internal tandem duplication (ITD) in exon 15 of *BCOR* on Xp11.4. In the schematic diagram, the parental segment (P) that is duplicated is depicted in blue and the ITD segment is indicated in red. The parental segment sequences of the ITD are shown at the bottom.

BCOR exon 15 and *CCNB3* intron 4, producing an in-frame chimeric transcript (**Figure 5B**). Based on this finding, the final diagnosis of case 2 was revised as '*BCOR-CCNB3* gene fusion-positive round cell sarcoma arising in bone'. In case 4, RNA-seq did not detect any specific gene fusion, however additional WGS analysis identified *BCOR* exon 15-ITD (**Figure 6**), the classic genetic characteristic of CCSK. Therefore, case 4 with typical morphological phenotype and genetic feature of CCSK, was finally diagnosed as 'a soft tissue counterpart of CCSK'. No fusion transcripts or specific gene abnormalities were identified in the other 3 cases.

Discussion

At present, detection of specific genetic alterations by next-generation sequencing technology might be pivotal in refining the diagnosis and classification of URCSs that display ambiguous morphologic and immunophenotypic features. In this study, we identified a round cell sarcoma in bone harboring *BCOR-CCNB3* fusion gene by RNA-seq and an infantile soft tissue round cell sarcoma with *BCOR*-ITD by WGS.

Chromosome rearrangements involving *BCOR* have been detected in URCSs (including *BCOR-CCNB3, BCOR-MAML3,* and *ZC3H7B-BCOR*) [2, 7], endometrial stromal sarcoma (*ZC3H7B-BCOR*) [8, 9], ossifying fibromyxoid tumor (*ZC3H7B-BCOR*) [10], and acute myeloid leukemia (*BCOR-RARα*) [11]. These results indicate *BCOR*-rearranged sarcomas occur predominantly in males, preferentially distribute within bones of adolescents and young adults (median age at diagnosis, 13 years) and tend to present a potentially less aggressive clinical course than classic ES [2, 3, 12]. *BCOR* exon 15 ITD has also been previously identified as a recurrent somatic mutation in a subset of CCSK [13], infantile URCS [14], primitive myxoid mesenchymal tumor of infancy [15], and a subset of central nervous system-high grade neuroepithelial tumors [16]. CCSK is a sarcoma which occurs preferentially in the kidney of young children [17, 18]. Histologically, CCSK is composed of round to short shuttle-like cells with pale chromatin and indistinct nucleoli, a prominent capillary network, extensive myxoid stroma with microcyst formation. Immunohistochemically, CCSK shows diffuse cyclin D1 expression [19]. Genetically, CCSK is characterized as harboring either *BCOR*-ITD in the majority of cases (approximately 85%) or *YWHAE-NUTM-2B/E* fusion in a minority of cases [13, 20, 21]. Extra-renal CCSK with the two genetic hallmarks has been reported [14]. Moreover, the cases of primary renal sarcomas with *BCOR-CCNB3* gene fusion have been reported and interestingly, these renal sarcomas do overlap with CCSK at the phenotype and genetic level [19, 22].

In consistent with the above clinicopathological data, the *BCOR-CCNB3* positive round cell sarcoma in our study occurred in the sacrum of a 17-year-old male patient, and immunohistochemistry staining showed the tumor cells had a far lower Ki-67 proliferation index (about 10%) than ES (about 80%). However, the soft tissue round cell sarcoma with *BCOR*-ITD occurred in the groin of a 7-month-old infant in contrast to onset ages of *BCOR-CCNB3* sarcoma and renal CCSK which presented a broader age range at diagnosis. The age at presentation of this case was in keeping with the observations from Kao YC et al. [14].

Microscopically, the *BCOR-CCNB3* gene fusion-positive sarcoma (case 2) displayed morphologic features overlapping with the sarcoma with *BCOR*-ITD (case 4), including alternating hypercellular and hypocellular areas, a mixture

of round cell and focal spindle cells components, pale nuclear chromatin, indistinct nucleoli, and abundant myxoid matrix. Both sarcomas diffusely and strongly expressed cyclin D1, the recognized marker of CCSK, supporting the potential overlap with CCSK. Two cases showed similar expression pattern and staining intensity for CD99 (both diffuse and relatively strong staining pattern) and CD56 (both patchy and weak staining pattern). In both cases, Ki-67 staining displayed a low proliferation index (about 10%) suggesting that the tumor with *BCOR*-ITD or *BCOR-CCNB3* might have a less aggressive clinical course in contrast to Ewing sarcoma. Additionally in case 4, we observed some morphologic features reminiscent of CCSK appearance, including a delicate arborizing vascular network, focal microcyst formation and cellular fibrous septa, which were not found in case 2. Thus, although there was obvious morphologic similarity between case 2 and case 4, but case 4 shared more morphologic overlap with classic appearance of CCSK.

Previous studies have highlighted that there was a morphology and transcriptional profile overlap among *BCOR*-ITD-positive URCSs/primitive myxoid mesenchymal tumor of infancy (PMMTI), *BCOR-CCNB3* fusion-positive sarcoma and CCSK [14]. Argani P et al. further proposed the concept of "*BCOR*-alteration family" that the CCSK, URCSs/PMMTI harboring *BCOR*-ITD, and *BCOR-CCNB3* sarcomas can be regarded as the same pathologic subclassification owing to overlapping clinicopathologic features and a common genetic signature [22]. In the previous reports, most infantile URCSs harboring *BCOR*-ITD were composed of sheets or lobules of monotonous small round cells [14], whereas *BCOR-CCNB3* sarcomas were uniformly high cellularity and were composed of monomorphic round or spindle cells which overlapped with ES or synovial sarcoma [22]. However, the two sarcomas involving *BCOR* abnormalities reported by us microscopically demonstrated a heterogeneous appearance that hypercellular areas alternated with less cellular areas and round cell components admixed with focal spindle cells. These features also appeared in the cases of *BCOR-CCNB3* fusion-positive sarcomas reported by Peters TL et al. [12]. It is worth mentioning that the transcripts identified by us show a fusion of the *BCOR* exon 15 to *CCNB3* intron 4, not exactly the same as the previous reports that the *BCOR* exon 15 is often fused to *CCNB3* exon 5 [2, 12]. Regretfully, neither of the two cases with gene abnormalities involving *BCOR* had tissue available for mRNA expression analysis.

Furthermore, there were morphologic similarities between case 1 and case 3 and both tumors were composed of solid sheets of tumor cells with vesicular nuclei and occasional small nucleoli. Also, case 5 had histopathologic overlap with the control case (ES), that was presented as monotonous small blue round cells with scant cytoplasm and hyperchromatic nuclei and abundant collagenized stroma. However, the current research failed to classify them accurately.

In summary, our finding showed that the round cell sarcoma with *BCOR-CCNB3* fusion shared morphologic features with *BCOR*-ITD positive sarcoma, the latter being more definitely referred to as 'counterpart of CCSK in soft tissue'. Additional investigations are required to analyze the link among histopathologic features, molecular biologic functions and genetic aberration in this tumor subgroup. With increasing awareness of the distinct tumor entity harboring *BCOR* alteration and its morphologic characteristics, combined with the elevating availability of next-generation sequencing, it is probably that such tumors will be readily diagnosed in the foreseeable future, thus providing sufficient cases for further studies to determine the clinical behavior, prognosis and targeted therapy.

Acknowledgements

This work was supported by 2 grants from the National Natural Science Foundation of China (81772862 and 81402413).

Disclosure of conflict of interest

None.

Address correspondence to: Dr. Anjia Han, Department of Pathology, The First Affiliated Hospital, Sun Yat-sen University, No. 58, Zhongshan Road II, Guangzhou 510080, Guangdong, P. R. China. Tel: 8620-87332235; Fax: 8620-87-332235; E-mail: hananjia@mail.sysu.edu.cn

References

[1] Fletcher CDM, Chibon F, Mertens F. WHO classification of tumours of soft tissue and bone.

In: Fletcher CDM, Bridge JA, Hogendoorn PCW, Mertens F, editors. Undifferentiated/unclassified sarcomas. 4th, edition. IARC. Lyon; 2013. pp. 235-8.

[2] Pierron G, Tirode F, Lucchesi C, Reynaud S, Ballet S, Cohen-Gogo S, Perrin V, Coindre JM, Delattre O. A new subtype of bone sarcoma defined by BCOR-CCNB3 gene fusion. Nat Genet 2012; 44: 461-466.

[3] Puls F, Niblett A, Marland G, Gaston CL, Douis H, Mangham DC, Sumathi VP, Kindblom LG. BCOR-CCNB3 (Ewing-like) sarcoma: a clinicopathologic analysis of 10 cases, in comparison with conventional Ewing sarcoma. Am J Surg Pathol 2014; 38: 1307-1318.

[4] Choi EY, Thomas DG, McHugh JB, Patel RM, Roulston D, Schuetze SM, Chugh R, Biermann JS, Lucas DR. Undifferentiated small round cell sarcoma with t(4;19) (q35;q31.1) CIC-DUX4 fusion: a novel highly aggressive soft tissue tumor with distinctive histolopathology. Am J Surg Pathol 2013; 37: 1379-1386.

[5] Yoshida A, Goto K, Kodaira M, Kobayashi E, Kawamoto H, Mori T, Yoshimoto S, Endo O, Kodama N, Kushima R, Hiraoka N, Motoi T, Kawai A. CIC-rearranged sarcomas: a study of 20 cases and comparisons with Ewing sarcomas. Am J Surg Pathol 2016; 40: 313-323.

[6] Donahue JE, Yakirevich E, Zhong S, Treaba DO, Lakis NS, Ali SM, de la Monte SM, Mangray S. Primary spinal epidural CIC-DUX4 undifferentiated sarcoma in a child. Pediatr Dev Pathol 2018; 21: 411-417.

[7] Specht K, Zhang L, Sung YS, Nucci M, Dry S, Vaiyapuri S, Richter GH, Fletcher CD, Antonescu CR. Novel BCOR-MAML3 and ZC3H7B-BCOR gene fusions in undifferentiated small blue round cell sarcomas. Am J Surg Pathol 2016; 40: 433-442.

[8] Panagopoulos I, Thorsen J, Gorunova L, Haugom L, Bjerkehagen B, Davidson B, Heim S, Micci F. Fusion of the ZC3H7B and BCOR genes in endometrial stromal sarcomas carrying an X;22-translocation. Genes Chromosomes Cancer 2013; 52: 610-618.

[9] Hoang LN, Aneja A, Conlon N, Delair DF, Middha S, Benayed R, Hensley ML, Park KJ, Hollmann TJ, Hameed MR, Antonescu CR, Soslow RA, Chiang S. Novel high-grade endometrial stromal sarcoma: a morphologic mimicker of myxoid leiomyosarcoma. Am J Surg Pathol 2017; 41: 12-24.

[10] Antonescu CR, Sung YS, Chen CL, Zhang L, Chen HW, Singer S, Agaram NP, Sboner A, Fletcher CD. Novel ZC3H7B-BCOR, MEAF6-PHF1, and EPC1-PHF1 fusions in ossifying fibromyxoid tumors--molecular characterization shows genetic overlap with endometrial stromal sarcoma. Genes Chromosomes Cancer 2014; 53: 183-193.

[11] Yamamoto Y, Tsuzuki S, Tsuzuki M, Handa K, Inaguma Y, Emi N. BCOR as a novel fusion partner of retinoic acid receptor alpha in a t(X;17) (p11;q12) variant of acute promyelocytic leukemia. Blood 2010; 116: 4274-4283.

[12] Peters TL, Kumar V, Polikepahad S, Lin FY, Sarabia SF, Liang Y, Wang WL, Lazar AJ, Doddapaneni H, Chao H, Muzny DM, Wheeler DA, Okcu MF, Plon SE, Hicks MJ, López-Terrada D, Parsons DW, Roy A. BCOR-CCNB3 fusions are frequent in undifferentiated sarcomas of male children. Mod Pathol 2015; 28: 575-586.

[13] Ueno-Yokohata H, Okita H, Nakasato K, Akimoto S, Hata J, Koshinaga T, Fukuzawa M, Kiyokawa N. Consistent in-frame internal tandem duplications of BCOR characterize clear cell sarcoma of the kidney. Nat Genet 2015; 47: 861-863.

[14] Kao YC, Sung YS, Zhang L, Huang SC, Argani P, Chung CT, Graf NS, Wright DC, Kellie SJ, Agaram NP, Ludwig K, Zin A, Alaggio R, Antonescu CR. Recurrent BCOR internal tandem duplication and YWHAE-NUTM2B fusions in soft tissue undifferentiated round cell sarcoma of infancy: overlapping genetic features with clear cell sarcoma of kidney. Am J Surg Pathol 2016; 40: 1009-1020.

[15] Santiago T, Clay MR, Allen SJ, Orr BA. Recurrent BCOR internal tandem duplication and BCOR or BCL6 expression distinguish primitive myxoid mesenchymal tumor of infancy from congenital infantile fibrosarcoma. Mod Pathol 2017; 30: 884-891.

[16] Sturm D, Orr BA, Toprak UH, Hovestadt V, Jones DTW, Capper D, Sill M, Buchhalter I, Northcott PA, Leis I, Ryzhova M, Koelsche C, Pfaff E, Allen SJ, Balasubramanian G, Worst BC, Pajtler KW, Brabetz S, Johann PD, Sahm F, Reimand J, Mackay A, Carvalho DM, Remke M, Phillips JJ, Perry A, Cowdrey C, Drissi R, Fouladi M, Giangaspero F, Łastowska M, Grajkowska W, Scheurlen W, Pietsch T, Hagel C, Gojo J, Lötsch D, Berger W, Slavc I, Haberler C, Jouvet A, Holm S, Hofer S, Prinz M, Keohane C, Fried I, Mawrin C, Scheie D, Mobley BC, Schniederjan MJ, Santi M, Buccoliero AM, Dahiya S, Kramm CM, von Bueren AO, von Hoff K, Rutkowski S, Herold-Mende C, Frühwald MC, Milde T, Hasselblatt M, Wesseling P, Rößler J, Schüller U, Ebinger M, Schittenhelm J, Frank S, Grobholz R, Vajtai I, Hans V, Schneppenheim R, Zitterbart K, Collins VP, Aronica E, Varlet P, Puget S, Dufour C, Grill J, Figarella-Branger D, Wolter M, Schuhmann MU, Shalaby T, Grotzer M, van Meter T, Monoranu CM, Felsberg J, Reifenberger G, Snuderl M, Forrester LA, Koster J, Versteeg R, Volckmann R, van Sluis P, Wolf S, Mikkelsen T, Gajjar A, Aldape K, Moore AS, Taylor MD, Jones C, Jabado N, Karajannis MA, Eils R, Schlesner M, Lichter P, von Deimling A, Pfister SM, Ellison

DW, Korshunov A, Kool M. New brain tumor entities emerge from molecular classification of CNS-PNETs. Cell 2016; 164: 1060-1072.

[17] Argani P, Perlman EJ, Breslow NE, Browning NG, Green DM, D'Angio GJ, Beckwith JB. Clear cell sarcoma of the kidney: a review of 351 cases from the national wilms tumor study group pathology center. Am J Surg Pathol 2000; 24: 4-18.

[18] Gooskens SL, Furtwängler R, Vujanic GM, Dome JS, Graf N, van den Heuvel-Eibrink MM. Clear cell sarcoma of the kidney: a review. Eur J Cancer 2012; 48: 2219-2226.

[19] Wong MK, Ng CCY, Kuick CH, Aw SJ, Rajasegaran V, Lim JQ, Sudhanshi J, Loh E, Yin M, Ma J, Zhang Z, Iyer P, Loh AHP, Lian DWQ, Wang S, Goh SGH, Lim TH, Lim AST, Ng T, Goytain A, Loh AHL, Tan PH, Teh BT, Chang KTE. Clear cell sarcomas of the kidney are characterised by BCOR gene abnormalities, including exon 15 internal tandem duplications and BCOR-CCNB3 gene fusion. Histopathology 2018; 72: 320-329.

[20] O'Meara E, Stack D, Lee CH, Garvin AJ, Morris T, Argani P, Han JS, Karlsson J, Gisselson D, Leuschner I, Gessler M, Graf N, Fletcher JA, O'Sullivan MJ. Characterization of the chromosomal translocation t(10;17) (q22;p13) in clear cell sarcoma of kidney. J Pathol 2012; 227: 72-80.

[21] Karlsson J, Valind A, Gisselsson D. BCOR internal tandem duplication and YWHAE-NUTM2B/E fusion are mutually exclusive events in clear cell sarcoma of the kidney. Genes Chromosomes Cancer 2016; 55: 120-123.

[22] Argani P, Kao YC, Zhang L, Bacchi C, Matoso A, Alaggio R, Epstein JI, Antonescu CR. Primary renal sarcomas with BCOR-CCNB3 gene fusion: a report of 2 cases showing histologic overlap with clear cell sarcoma of kidney, suggesting further link between BCOR-related sarcomas of the kidney and soft tissues. Am J Surg Pathol 2017; 41: 1702-1712.

Supplementary Protocols

Fluorescence in situ hybridization (FISH)

Dual color FISH was performed on interphase nuclei to identify the presence of some known gene rearrangements using *EWSR1*, *SYT* and *FUS* break-apart probes (Vysis LSI® EWSR1 (22q12) Dual Color, Break Apart Rearrangement Probe; Vysis LSI® SS18 (18q11.2) Dual Color, Break Apart Rearrangement Probe; Vysis LSI® FUS (16p11) Dual Color, Break Apart Rearrangement Probe). Briefly, 4-μm formalin-fixed paraffinembedded (FFPE) tissue sections from all 6 cases were mounted on charged slides. A serial H&E-stained slides were used to identify tumoral tissues. The unstained slides were deparaffinized, subjected to 2 25-minute rounds of pepsin digestion at 37°C, dehydrated in 70%, 95%, and 100% ethanol for 2 minutes each, and air dried. Probe (3 μL) was applied to each slide, followed by denaturation of the probe and target at 80°C for 5 minutes and overnight hybridization at 37°C. The slides were then washed in 2× standard sodium citrate for 2 minutes twice at 37°C, stained with DAPI, and mounted with anti-fade solution. For each slide, 200 successive cells were scored using an Olympus BX51 fluorescent microscope (Tokyo, Japan), controlled by IMSTAR software (Paris, France). Gene rearrangement was reported as present if >20% of the tumor nuclei showed split signals defined as separation of signals. Nuclei with incomplete sets of signals were omitted from the score.

Fusion detection of RNA-seq data

Three tools were applied for fusion detection of RNA-seq data. FusionCatcher (verison 0.99.4e) was used with parameters (--aligners blat, otherwise default parameter) which uses Bowtie aligner to perform both transcriptome and genome mapping and then uses BLAT aligner to further map unmapped reads and count fusion supporting evidence. The other two tools namely Factera and Socrates (https://github.com/jibsch/Socrates) were both executed using default parameters. Specially, Socrates takes the modified BAM file, which converted hard-clip in original BAM into soft-clip to improve the fusion detection performance. The combined fusion results from all tools were manually reviewed on IGV for confirmation.

Whole genome sequencing (WGS)

Genomic DNA from FFPE sample was extracted using the QIAamp DNA FFPE Tissue Kit (Qiagen). Purified DNA was qualified by Nanodrop2000 (Thermo Fisher Scientific) and quantified by Qubit 3.0 using the dsDNA HS Assay Kit (Life Technologies) according to the manufacturer's recommendations. Sequencing libraries were prepared using the KAPA Hyper Prep kit (KAPA Biosystems) with an optimized manufacturer's protocol. In brief, 1 μg of genomic DNA, which was sheared into 350 bp fragments using the Covaris M220 instrument (Covaris), underwent end-repairing, A-tailing and ligation with indexed adapters sequentially, followed by size selection using Agencourt AMPure XP beads (Beckman Coulter). Finally, libraries were amplified by 4 cycles of PCR and purified using Agencourt AMPure XP beads. Each library was quantified by qPCR using the KAPA Library Quantification kit (KAPA Biosystems). Library fragment size was determined by the Agilent Technologies 2100 Bioanalyzer (Agilent), and was then sequenced on HiSeqX-TEN NGS platforms (Illumina) according to the manufacturer's instructions. Sequencing data generated through Illumina sequencing platform was converted to fastq format and demultiplexed using bcl2fastq. Paired-end sequencing reads were then aligned to human reference genome GRCh37/hg19 downloaded UCSC genome browser using Burrows-Wheeler Aligner (bwa-mem, version 0.7.12-r1039). Aligned reads were sorted using Picard (version 1.119) (available at: http://broadinstitute.github.io/picard). The output BAM files were further processed using Picard to remove duplicates. Realignment and recalibration was performed using the Genome Analysis Tool Kit (GATK, version 3.6) using the RealignerTargetCreator, IndelRealigner, BaseRecalibrator, and PrintReads modules. Variants were called using the HaplotypeCaller module available in the GATK. We used the following criteria to filter the resulting single nucleotide variants (SNV) and short insertion/deletion mutations (Indel) obtained from the previous step: 1) the mutation sites should have a minimum sequencing depth of 6X; 2) the quality score of the supporting base calling should be no less than Q20; 3) the detected mutation should have a minimum variant allelic frequency (VAF) of 10%; 4) the detected mutation should be supported by no less than 2 sequencing reads; 5) the detected mutation should have a mutation quality score (as determined by GATK) no less than 30.

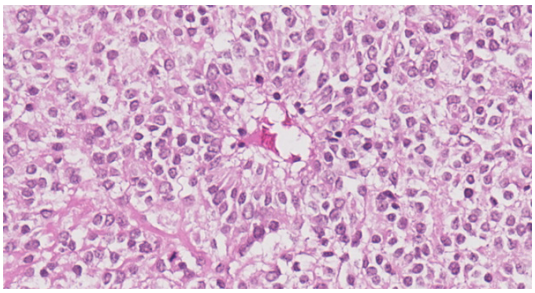

Supplementary Figure 1. Formation of vascular pseudorosette in case 3 (400×).

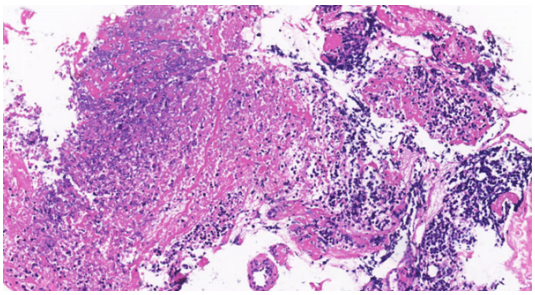

Supplementary Figure 2. Foci of necrosis in case 5 (100×).

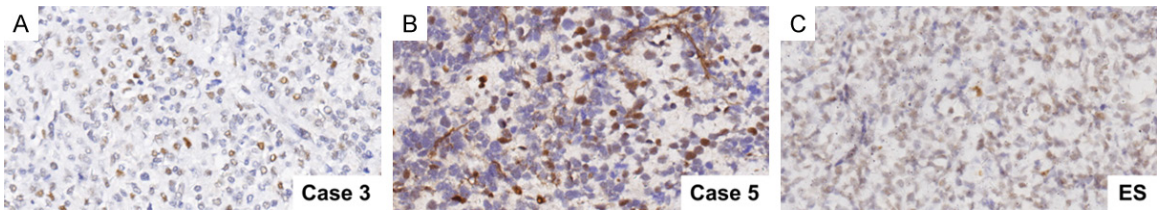

Supplementary Figure 3. Positive cases for nuclear Fli-1 expression. (A, B) Immunohistochemistry staining demonstrated scattered nuclear Fli-1 expression in 2 URCSs, being weak-to-moderate intensity in case 3 (A, 400×) and moderate-to-strong in case 5 (B, 400×). (C) Diffuse but weak nuclear Fli-1 expression was detected in ES (400×).

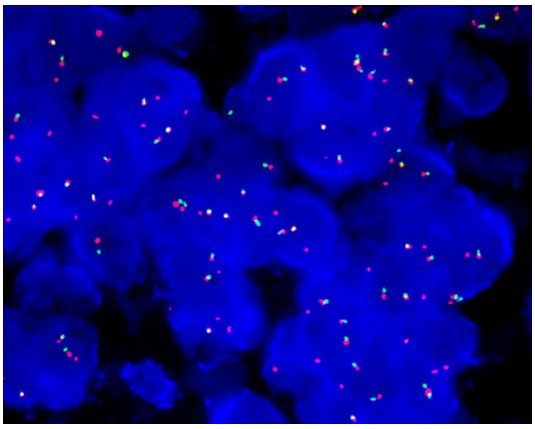

Supplementary Figure 4. FISH detection of *EWSR1* rearrangements in ES. *EWSR1* rearrangement confirmed by separation of green (telomeric) and red (centromeric) FISH probe signals flanking the *EWSR1* gene.